Phase Transitions in Shear-Induced Segregation of Granular Materials

Yi Fan and K. M. Hill

St. Anthony Falls Laboratory, Department of Civil Engineering, University of Minnesota, Minneapolis, Minnesota 55414, USA

(Received 7 January 2011; published 27 May 2011)

We computationally study shear-induced segregation of different-sized particles in vertical chute flow. We find that, for low solid fractions, large particles segregate toward regions of low shear rates where the granular temperature (velocity variance) is low. As the solid fraction increases, this trend reverses, and large particles segregate toward regions of high shear rates and temperatures. We find that this is a global phenomenon: local segregation trends reverse at high system solid fractions even where local solid fractions are small. The reversal corresponds to the growth of a single enduring cluster of 30%–60% of the particles that we propose changes the segregation dynamics.

DOI: 10.1103/PhysRevLett.106.218301 PACS numbers: 47.57.Gc, 45.70.Mg, 81.05.Rm

Granular mixtures of particles differing in size, density, or other particle property tend to demix or segregate into often brilliant patterns. This gives rise to a number of interesting pattern formation problems in nature [1] and challenges for powder processing industries [2]. Several different factors influence segregation behaviors, including gravity, gradients of shear rates, and granular temperature (velocity variance) T. Of these, segregation associated with gravity has been studied the most [3–6], though this is often accompanied by shear rate gradients. The influence of shear rate gradients on segregation, particularly for denser configurations, is much less understood [7].

Shear rate gradients drive gradients in T as well as gradients in the solid fraction f. In sheared dilute energetic granular mixtures all particles accumulate in the regions of low shear rate $\dot{\gamma}$ corresponding to regions of low T and high f, and larger particles do so more efficiently (e.g., [8–11]), leaving the latter segregated at the regions of lowest $\dot{\gamma}$ and T, as well as highest f. This has been successfully modeled using kinetic theory [8,11–14] for sufficiently sparse flows. For moderate solid fractions, kinetic theory has been shown to overpredict segregation trends, though still qualitatively reproduce the outcome [10]. For sufficiently high solid fractions f, there is evidence the segregation trend reverses, that larger particles segregate to regions of higher shear rates and higher T's [15,16], though the evidence was obtained primarily from systems where simultaneous advection complicated the outcome. When complex advection combines with even relatively simple segregation tendencies, the underlying mechanisms are hard to discern [16].

In this Letter, we investigate segregation associated with a shear rate gradient as it varies with the system solid fraction $\langle \bar{f} \rangle$ [17]. We use a vertical chute [Fig. 1(a)] to isolate the effect of a shear rate gradient on segregation. As shown for other shear-induced effects [18–20], this geometry is ideal for studying the effect of shear rate gradients on segregation because of its simple geometry but inhomogeneous flow structure. We find that while the local solid fraction $\bar{f}$ and other kinematics are nonuniform, the segregation trend varies with the global solid fraction $\langle \bar{f} \rangle$. For systems of low $\langle \bar{f} \rangle$, large particles accumulate within low-$\dot{\gamma}$, low-T, high-f regions, in quantitative agreement with predictions using kinetic theory. However, for systems of high $\langle \bar{f} \rangle$, the opposite occurs, and our attempt to match kinetic theory with our results fails dramatically. We find this change in segregation behavior is associated with the system structure: as $\langle \bar{f} \rangle$ increases, the system structure changes from one dominated by binary collisions to one dominated by one cluster that can involve >60% of the particles and span the system. As such, the cluster size may be an order parameter characterizing a phase change of the system of which the segregation behavior is a signature.

For our simulations we use the discrete element method [21] in three dimensions. Particle-particle and particle-wall

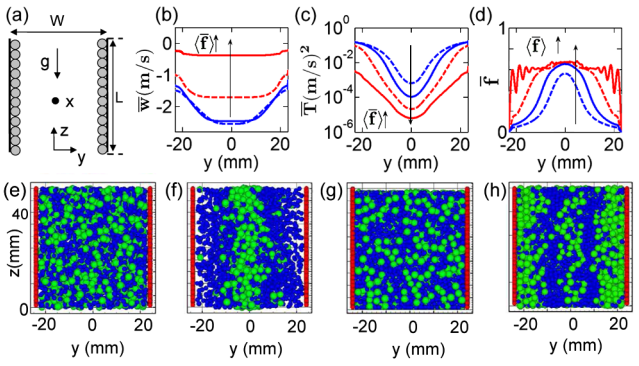

FIG. 1 (color online). (a) Sketch of a vertical chute. (b)–(d) Profiles of kinematic quantities for four mixtures once steady state is reached ($t = 50$ s for $\langle \bar{f} \rangle = 0.21$ and 0.34 and $t = 400$ s for $\langle \bar{f} \rangle = 0.47$ and 0.60). (b) Average streamwise velocity $\bar{w}$, (c) average granular temperature $\bar{T}$, and (d) average solid fraction of the mixture $\bar{f}$. (e)–(h) Snapshots of two mixtures at $t = 0$ s and steady state. (e) $\langle \bar{f} \rangle = 0.21$ at $t = 0$ s, (f) $\langle \bar{f} \rangle = 0.21$ at $t = 50$ s, (g) $\langle \bar{f} \rangle = 0.60$ at $t = 0$ s, and (h) $\langle \bar{f} \rangle = 0.60$ at $t = 400$ s. Two millimeter particles, blue (dark); 3 mm particles, green (light).

contact forces are represented using a nonlinear force model based on Hertzian and Mindlin contact theories and damping components based on the derivation in Tsuji, Tanaka, and Ishida [22,23]. The contact forces also obey the Coulomb law of friction. For the results described here, we use 50/50 mixtures (by weight) of spherical particles 2 and 3 mm in diameter with a polydispersity of 10% to impede crystallization. We vary $\langle \bar{f} \rangle$ from one simulation to the next: $\langle \bar{f} \rangle = 0.21$–$0.60$. (The number of particles in each simulation N varies from 2976 to 8089.) The boundary conditions we use are those of a vertical chute of dimensions $D = 40$ mm, $W = 50$ mm, and $L = 50$ mm in the x, y, and z directions, respectively [see Fig. 1(a)]. The boundaries are periodic in the z (vertical) and x directions. There is one set of vertical side walls (in the y direction) that are roughened using close-packed 2 mm spheres. We denote the velocity and components as $\mathbf{u} = u\mathbf{x} + v\mathbf{y} + w\mathbf{z}$ according to directions noted in Fig. 1(a).

For each simulation, the particles are arranged randomly in the chute and then released with small random velocities. After their release, particles collide with one another and with the vertical walls as they accelerate downward. Dissipation of energy via interparticle and wall-particle interactions limits the velocity throughout the cell. Steady-state velocities are reached within ~10 s. The steady-state kinematic profiles of the granular mixtures are similar to those in a monosized system measured in the physical and computational experiments (e.g., Refs. [18,19,24]). At the highest solid fractions, the vertical velocity profile $\bar{w}$ resembles a plug flow; at the lower solid fractions, the velocity is higher and the profile is roughly parabolic [Fig. 1(b)]. In all cases, the granular temperature $\bar{T}$ is highest near the walls where the shear rate $\dot{\gamma} = d\bar{w}/dy$ is the greatest, and generally higher for lower values of $\langle \bar{f} \rangle$ [Fig. 1(c)]. Regions of low $\bar{T}$ and low $\dot{\gamma}$ correspond to regions of high $\bar{f}$ [Fig. 1(d)].

We find that segregation in our sparsest simulations proceeds similarly to segregation reported in other sparse systems (e.g., [8,11]). All particles move to regions of low $\bar{T}$, low $\dot{\gamma}$, and high $\bar{f}$ in the center of the chute, though large particles do so more efficiently [see Figs. 1(e) and 1(f)]. In contrast, in our densest simulations, the larger particles segregate to the region of high $\bar{T}$ and $\dot{\gamma}$ near the walls [see Figs. 1(g) and 1(h)]. To investigate these trends more quantitatively, we plot the solid fraction profiles $\bar{f}_i$ of each component i and the mixture $\bar{f}$ for the steady state for three representative solid fractions—$\langle \bar{f} \rangle = 0.21$, 0.47, 0.60—in Fig. 2, row 1. These plots indicate a gradual change: as $\langle \bar{f} \rangle$ increases, the large particles are increasingly repelled from the central region of low $\bar{T}$ and $\dot{\gamma}$ to the regions of high $\bar{T}$ and $\dot{\gamma}$ at the boundaries. For the systems with the highest values of $\langle \bar{f} \rangle$, the segregation in the center is quite small, apparently due to the slow dynamics in the center of the flow.

To investigate the dynamics that give rise to these steady-state concentrations, we plot the normalized

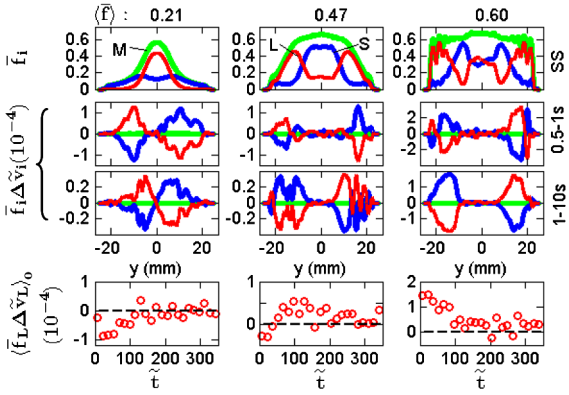

FIG. 2 (color online). Segregation kinematics of three systems with $\langle \bar{f} \rangle$'s as noted for the mixture (M) [green (light gray line)] and large (L) [red (thin dark gray line)] and small (S) [blue (thick dark gray line)] particles. Row 1: $\bar{f}_i(y)$ at steady state (SS). Rows 2 and 3: normalized segregation fluxes $\bar{f}_i \Delta\tilde{v}_i(y)$ as defined in text averaged over $t = 0.5$–1 s (row 2) and 1–10 s (row 3). Row 4: normalized net outward average segregation fluxes for large particles $\langle \bar{f}_L \Delta\tilde{v}_L \rangle_o$ as a function of normalized time $\tilde{t}$.

segregation flux for these systems $\bar{f}_i \Delta\tilde{v}_i = \bar{f}_i(\bar{v}_i - \bar{v})/\langle \bar{w} \rangle$ where $\langle \bar{w} \rangle$ is the steady-state spatially averaged vertical velocity. We find that immediately following the release of the particles ($t = 0.5$–1 s) the large particles segregate to the center of the cell for all cases except for the highest solid fractions investigated (e.g., $\langle \bar{f} \rangle = 0.60$ in Fig. 2, row 2). However, when these dynamics are viewed over a slightly longer period of time ($t = 1$–10 s), the segregation flux reversal occurs at moderate $\langle \bar{f} \rangle$'s (e.g., $\langle \bar{f} \rangle = 0.47$ in Fig. 2, row 3). We note this reversal occurs for moderate-to-high $\langle \bar{f} \rangle$'s even where the local value of $\bar{f}$ is relatively low. To calculate an average measure of segregation of each component i toward high-$\bar{T}$, high-$\dot{\gamma}$ regions, we compute the average flux of each component toward the walls: $\langle \bar{f}_i \Delta\tilde{v}_i \rangle_o \equiv \langle \bar{f}_i \Delta\tilde{v}_i \rangle_{y>0} - \langle \bar{f}_i \Delta\tilde{v}_i \rangle_{y<0}$. In Fig. 2, row 4, we plot average net outward segregation fluxes of large particles $\langle \bar{f}_L \Delta\tilde{v}_L \rangle_o$ vs normalized time $\tilde{t} = t\langle \bar{w} \rangle/W$ for the three systems discussed above. The results illustrate that the segregation of large particles toward low-$\bar{T}$, low-$\dot{\gamma}$ regions at $\langle \bar{f} \rangle = 0.21$ occurs at roughly the same (nondimensionalized) rate as the segregation of large particles toward high-$\bar{T}$, high-$\dot{\gamma}$ regions at $\langle \bar{f} \rangle = 0.60$. Further, in the intermediate system $\langle \bar{f} \rangle = 0.47$, the crossover from $\langle \bar{f}_L \Delta\tilde{v}_L \rangle_o < 0$ to $\langle \bar{f}_L \Delta\tilde{v}_L \rangle_o > 0$ at $\tilde{t} \approx 50$ is clearly indicated.

For physical insight, we compare our data with predictions from kinetic theory with nonequipartition of granular temperature [11,13], summarized in Ref. [16]. Specifically, we consider the "diffusion velocity," $\delta v \equiv \bar{v}_S - \bar{v}_L$. Figure 3 contains theoretical predictions of δv vs y based on local kinematics and simulation results for a few values of $\langle \bar{f} \rangle$ for $t = 0.5$–1 s. The results agree qualitatively and quantitatively for the lowest system solid fractions, e.g., $\langle \bar{f} \rangle = 0.21$ [Fig. 3(a)], though this agreement is not as good for higher $\langle \bar{f} \rangle$ as low as 0.34 [Fig. 3(b)]. Further, as shown

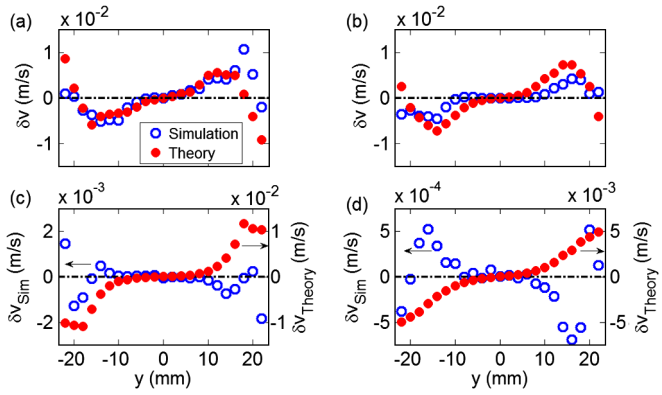

FIG. 3 (color online). Average segregation velocity $\delta v = \bar{v}_S - \bar{v}_L$ at 0.5–1 s from simulation results and from kinetic theory [11,13]. Derivation summarized in Ref. [16] for (a) $\langle \bar{f} \rangle = 0.21$, (b) $\langle \bar{f} \rangle = 0.34$, (c) $\langle \bar{f} \rangle = 0.55$, (d) $\langle \bar{f} \rangle = 0.60$.

in Figs. 3(c) and 3(d), in the denser systems, $\langle \bar{f} \rangle = 0.55$ and 0.60, the diffusion velocity predicted from kinetic theory is in the opposite direction (and significantly greater in magnitude) from that directly measured from the simulations. We found similar results at later times, though the qualitative disagreement between theory and simulation results occurs at lower values of $\langle \bar{f} \rangle$ where the segregation direction reverses.

Since current formulations of kinetic theory require collisions to be relatively uncorrelated, we hypothesize the change in segregation direction and the break between results and theory have to do with an underlying change in the structure of the system. To test this hypothesis, we consider a relatively coarse measure of the system structure, the size of particle clusters within each system. Here, we define the size of each cluster N_c by the number of particles connected via interparticle contacts [Fig. 4(a)]. Figures 4(b) and 4(c) show the probability distribution function (PDF) of the normalized cluster size N_c/N at steady state (using data from thousands of time steps) for different values of $\langle \bar{f} \rangle$. At lower values of $\langle \bar{f} \rangle$ [e.g., 0.21 in Fig. 4(b)] the clusters are very small, and the PDFs exhibit a power law decay. When $\langle \bar{f} \rangle$ increases to 0.37, the slope decreases and the tail of the PDF becomes more complicated. At higher values of $\langle \bar{f} \rangle$ [Fig. 4(c)], the PDF splits into two parts: one representing relatively small clusters that follows a power law, and one representing the size of the largest cluster N_{cm} at each time step. In Figs. 4(d) and 4(f), we plot the time dependence of N_{cm}/N. For the lowest value of $\langle \bar{f} \rangle = 0.21$, there is no unique largest cluster; many small clusters continuously form and break apart as mentioned. At $\langle \bar{f} \rangle = 0.37$, the largest cluster can reach 20%, though it is not stable and N_{cm}/N can vary from ~0.01 to 0.2, explaining the complicated tail in Fig. 4(b). For relatively large $\langle \bar{f} \rangle \geq 0.47$ there is a unique largest cluster that forms relatively quickly and contains a significant fraction of the particles, though for intermediate values, e.g., $\langle \bar{f} \rangle = 0.47$, the initial growth of the largest cluster is slow [Fig. 4(f)].

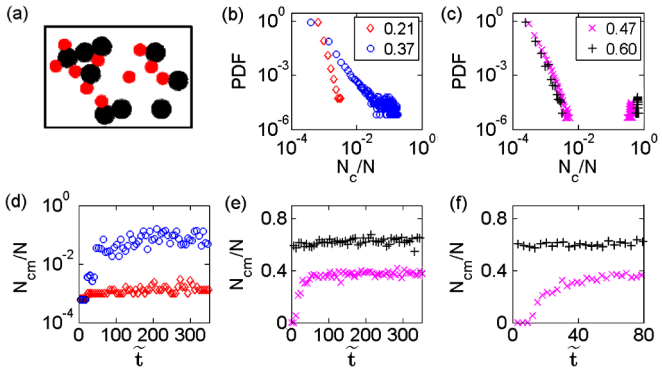

FIG. 4 (color online). (a) Sketch illustrating 4 clusters with 2 singletons. (b)–(c) Probability distribution function of N_c/N for (b) $\langle \bar{f} \rangle = 0.21$ and 0.37, and (c) $\langle \bar{f} \rangle = 0.47$ and 0.60. (d)–(e) Time dependence of the maximum cluster size for (d) $\langle \bar{f} \rangle = 0.21$ and 0.37, and (e)–(f) $\langle \bar{f} \rangle = 0.47$ and 0.60.

We now consider the correspondence between the growth of N_{cm}/N and the change in segregation trend with increasing $\langle \bar{f} \rangle$. We plot N_{cm}/N and $\langle \bar{f}_L \Delta \tilde{v}_L \rangle_o$ vs $\langle \bar{f} \rangle$ in Fig. 5. The results for $\langle \bar{f}_L \Delta \tilde{v}_L \rangle_o$ show the segregation flux transitions gradually from one where the large particles segregate toward low-$\bar{T}$, low-$\dot{\gamma}$ regions to the reverse, and that the transition point corresponds at early times to $\langle \bar{f} \rangle \sim 0.5$, and at later times to $\langle \bar{f} \rangle \sim 0.42$, as also suggested by Fig. 2. Further, it appears the reversal in segregation trends at early and late times coincides with a maximum cluster size somewhat greater than ~34% of the total number of particles and shifts to the left for slightly later times as N_{cm} grows.

To summarize, we find that the kinematics associated with shear rate gradients induce segregation for different-sized particles over a wide range of system solid fractions $\langle \bar{f} \rangle$ and that the direction of segregation of large particles relative to small particles reverses at a moderate value of $\langle \bar{f} \rangle$. The underlying cause for the reversal appears global; that is, local segregation trends reverse at higher $\langle \bar{f} \rangle$ even where local solid fractions are small. The transition is likely governed by the global structure of the system rather than a particular value of $\langle \bar{f} \rangle$. Indeed in the results reported in this Letter, we find the point of transition changes as the

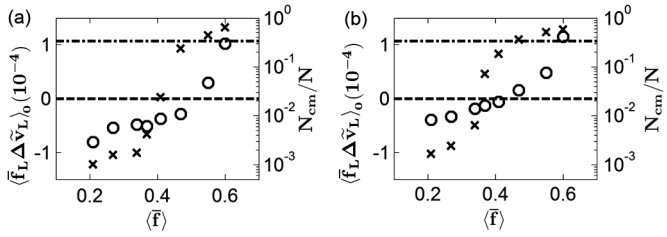

FIG. 5. $\langle \bar{f}_L \Delta \tilde{v}_L \rangle_o$ (○), and N_{cm}/N (×) vs $\langle \bar{f} \rangle$ calculated for (a) $t = 0.5$–1 s for $\langle \bar{f}_L \Delta \tilde{v}_L \rangle_o$ and $t = 0.75$ s for N_{cm}/N and (b) $t = 1$–10 s for $\langle \bar{f}_L \Delta \tilde{v}_L \rangle_o$ and $t = 5$ s for N_{cm}/N. The dashed line indicates $\langle \bar{f}_L \Delta \tilde{v}_L \rangle_o = 0$, and the dash-dotted line indicates $N_{cm}/N = 0.34$, the value for $\langle \bar{f} \rangle = 0.47$ at $\tilde{t} \approx 50$, the segregation reversal time indicated in Fig. 2, row 4.

system evolves to steady state. We further expect it to depend on details such as particle size distribution [25] as the maximum packing fraction changes. The size of the clusters we describe is likely related to an interparticle force correlation length ξ whose growth was shown by Lois Lemaître, and Carlson [26] to correspond with a transition from sparse to dense flow. They demonstrated that the transitional value of ξ depends on the interparticle restitution coefficient, which we expect will influence our segregation transition as well. While the current framework of kinetic theory does not correctly predict dynamics in highly correlated systems, efforts are being made to extend kinetic theory by explicitly incorporating a correlation length scale into the theory (e.g., Ref. [27]). Alternatively, a new model for segregation recently proposed by Sarkar and Khakhar for single-sized particles of different densities [28] shows promise as an alternate model for segregation in dense granular flows though it has not yet been applied to different-sized particles.

We conclude by considering a model proposed by Gray and colleagues for gravity-driven segregation of different-sized particles of identical material density ρ down a plane of inclination θ [4]. The model predicts that the segregation flux in the direction ζ perpendicular to the average flow should scale as $\sim \psi_i \partial\sigma/\partial\zeta - (f_i/f)\rho g \cos\theta$, where ψ_i is the fraction of the local pressure or normal stress σ born by species i. Essentially, gravity acts to drive all particles downward, and a nonequipartition of normal stress (where $\psi_i \neq f_i/f$) preferentially allows one species to respond more efficiently to $\partial\sigma/\partial\zeta$ than the other and thus segregates the particles. For sheared high $\langle\bar{f}\rangle$ systems where gravity does not play a role in segregation, we suggest explicit consideration of the contact stresses σ^c and kinetic stresses σ^k, associated with interparticle contacts and streaming motion of particles, respectively, as in Ref. [18]. Then, for a model analogous to that in Ref. [4] we suggest the segregation flux $\bar{f}_i \Delta\tilde{v}_i \sim \psi_i \partial\sigma^c_{yy}/\partial y + \psi^k_i \partial\sigma^k_{yy}/\partial y$ so that the negative kinetic stress gradient plays a role analogous to gravity. We are pursuing this framework for its potential to model shear-induced segregation in dense flows.

We thank Professors James Jenkins and Nico Gray for helpful discussions. We are grateful for the financial support of NSF CMS-0625022 and NSF CBET-0932735.

[1] J. M. N. T. Gray and B. P. Kokelaar, J. Fluid Mech. **652**, 105 (2010).
[2] T. Shinbrot and F. Muzzio, Phys. Today **53**, No. 3, 25 (2000).
[3] S. B. Savage and C. K. K. Lun, J. Fluid Mech. **189**, 311 (1988).
[4] J. M. N. T. Gray and A. R. Thornton, Proc. R. Soc. A **461**, 1447 (2005).
[5] D. V. Khakhar, J. J. McCarthy, and J. M. Ottino, Phys. Fluids **9**, 3600 (1997).
[6] J. T. Jenkins and D. K. Yoon, Phys. Rev. Lett. **88**, 194301 (2002).
[7] K. M. Hill and Y. Fan, Phys. Rev. Lett. **101**, 088001 (2008).
[8] S. L. Conway, X. Liu, and B. J. Glasser, Chem. Eng. Sci. **61**, 6404 (2006).
[9] J. Liu and A. D. Rosato, J. Phys. Condens. Matter **17**, S2609 (2005).
[10] H. Xu, M. Louge, and A. Reeves, Continuum Mech. Thermodyn. **15**, 321 (2003).
[11] J. E. Galvin, S. R. Dahl, and C. M. Hrenya, J. Fluid Mech. **528**, 207 (2005).
[12] J. T. Jenkins and F. Mancini, Phys. Fluids A **1**, 2050 (1989).
[13] D. K. Yoon and J. T. Jenkins, Phys. Fluids **18**, 073 303 (2006).
[14] D. V. Khakhar, J. J. McCarthy, and J. M. Ottino, Chaos **9**, 594 (1999).
[15] D. J. Stephens and J. Bridgwater, Powder Technol. **21**, 29 (1978).
[16] Y. Fan and K. M. Hill, Phys. Rev. E **81**, 041303 (2010).
[17] We use $\bar{*}$ to denote the temporal average of $*$, and $\langle * \rangle$ to denote the spatial average of $*$.
[18] V. Chikkadi and M. Alam, Phys. Rev. E **80**, 021303 (2009).
[19] K. S. Ananda, S. Moka, and P. R. Nott, J. Fluid Mech. **610**, 69 (2008); O. Pouliquen and R. Gutfraind, Phys. Rev. E **53**, 552 (1996).
[20] D. E. Liss, S. L. Conway, and B. J. Glasser, Phys. Fluids **14**, 3309 (2002); C. Denniston and H. Li, Phys. Rev. E **59**, 3289 (1999).
[21] P. A. Cundall and O. D. L. Strack, Geotechnique **29**, 47 (1979).
[22] We calculate the force between two objects according to $\mathbf{F} = F_n\mathbf{n} + F_t\mathbf{t}$; $\mathbf{n}$ and $\mathbf{t}$ are unit vectors normal and tangential to the contact plane, respectively; $F_n = k_n\delta_n^{3/2} + \eta_n\delta_n^{1/4}V_n$; $F_t = \min(k_t\delta_n^{1/2}\delta_t + \eta_t\delta_n^{1/4}V_t, \mu F_n)$, where δ_n and δ_t are normal and tangential overlaps between contacting objects; $k_{n,t}$, $\eta_{n,t}$, and μ are calculated using material properties as detailed in [23], though to save computational time we reduce k_n by a factor of $O(10^3)$, e.g., $(k_n, \eta_n, k_t, \eta_t)_{(2,2)} = (1.6 \times 10^6, 2.9 \times 10^{-1}, 2.1 \times 10^6, 3.3 \times 10^{-1})$, and $(k_n, \eta_n, k_t, \eta_t)_{(3,3)} = (1.7 \times 10^6, 3.7 \times 10^{-1}, 2.3 \times 10^6, 4.2 \times 10^{-1})$, where $(q)_{(i,j)}$ indicates coefficient q for contact between i and j mm particles. The units for $k_{n,t}$ are $\mathrm{N/m^{1.5}}$ and for $\eta_{n,t}$ are $\mathrm{N\,s/m^{1.25}}$. $\mu = 0.4$. (Sample simulations with and without reducing k_n indicate good agreement.)
[23] Y. Tsuji, T. Tanaka, and T. Ishida, Powder Technol. **71**, 239 (1992).
[24] GDRMiDi, Eur. Phys. J. E **14**, 341 (2004).
[25] B. Yohannes and K. M. Hill, Phys. Rev. E **82**, 061301 (2010).
[26] G. Lois, A. Lemaître, and J. M. Carlson, Phys. Rev. E **76**, 021302 (2007)
[27] J. Jenkins and D. Berzi, Granular Matter **12**, 151 (2010).
[28] S. Sarkar and D. V. Khakhar, Europhys. Lett. **83**, 54 004 (2008).